Diabetologia (2024) 67:1079–1094
https://doi.org/10.1007/s00125-024-06123-6

ARTICLE

Differential CpG methylation at *Nnat* in the early establishment of beta cell heterogeneity

Vanessa Yu[1] · Fiona Yong[1,2] · Angellica Marta[1] · Sanjay Khadayate[3] · Adrien Osakwe[4] · Supriyo Bhattacharya[5] · Sneha S. Varghese[6] · Pauline Chabosseau[1] · Sayed M. Tabibi[1] · Keran Chen[1,7] · Eleni Georgiadou[1] · Nazia Parveen[6] · Mara Suleiman[8] · Zoe Stamoulis[1,9] · Lorella Marselli[8] · Carmela De Luca[8] · Marta Tesi[8] · Giada Ostinelli[10] · Luis Delgadillo-Silva[10] · Xiwei Wu[5] · Yuki Hatanaka[3,11] · Alex Montoya[3] · James Elliott[3] · Bhavik Patel[3] · Nikita Demchenko[3,12] · Chad Whilding[3] · Petra Hajkova[3,11] · Pavel Shliaha[3] · Holger Kramer[3] · Yusuf Ali[13,14,15] · Piero Marchetti[8] · Robert Sladek[4,16] · Sangeeta Dhawan[6] · Dominic J. Withers[3,11] · Guy A. Rutter[1,10,2] · Steven J. Millership[1]

Received: 15 November 2023 / Accepted: 9 January 2024 / Published online: 21 March 2024
© The Author(s) 2024

Abstract

Aims/hypothesis Beta cells within the pancreatic islet represent a heterogenous population wherein individual sub-groups of cells make distinct contributions to the overall control of insulin secretion. These include a subpopulation of highly connected 'hub' cells, important for the propagation of intercellular Ca^{2+} waves. Functional subpopulations have also been demonstrated in human beta cells, with an altered subtype distribution apparent in type 2 diabetes. At present, the molecular mechanisms through which beta cell hierarchy is established are poorly understood. Changes at the level of the epigenome provide one such possibility, which we explore here by focusing on the imprinted gene *Nnat* (encoding neuronatin [NNAT]), which is required for normal insulin synthesis and secretion.

Methods Single-cell RNA-seq datasets were examined using Seurat 4.0 and ClusterProfiler running under R. Transgenic mice expressing enhanced GFP under the control of the *Nnat* enhancer/promoter regions were generated for FACS of beta cells and downstream analysis of CpG methylation by bisulphite sequencing and RNA-seq, respectively. Animals deleted for the de novo methyltransferase DNA methyltransferase 3 alpha (DNMT3A) from the pancreatic progenitor stage were used to explore control of promoter methylation. Proteomics was performed using affinity purification mass spectrometry and Ca^{2+} dynamics explored by rapid confocal imaging of Cal-520 AM and Cal-590 AM. Insulin secretion was measured using homogeneous time-resolved fluorescence imaging.

Results *Nnat* mRNA was differentially expressed in a discrete beta cell population in a developmental stage- and DNA methylation (DNMT3A)-dependent manner. Thus, pseudo-time analysis of embryonic datasets demonstrated the early establishment of *Nnat*-positive and -negative subpopulations during embryogenesis. NNAT expression is also restricted to a subset of beta cells across the human islet that is maintained throughout adult life. $NNAT^{+}$ beta cells also displayed a discrete transcriptome at adult stages, representing a subpopulation specialised for insulin production, and were diminished in *db/db* mice. 'Hub' cells were less abundant in the $NNAT^{+}$ population, consistent with epigenetic control of this functional specialisation.

Conclusions/interpretation These findings demonstrate that differential DNA methylation at *Nnat* represents a novel means through which beta cell heterogeneity is established during development. We therefore hypothesise that changes in

Vanessa Yu, Fiona Yong and Angellica Marta contributed equally to this study.

Guy A. Rutter and Steven J. Millership are joint senior authors.

Dr H. Kramer, who performed and interpreted experiments and analyses for this research, died on 23 August 2022 before publication of this work.

Extended author information available on the last page of the article

Research in context

What is already known about this subject?

- Neuronatin (*Nnat*/*NNAT*) is an imprinted gene in humans and mice and is required for glucose-stimulated insulin secretion in vivo
- Pancreatic beta cells are functionally heterogeneous with specific highly connected subpopulations known to coordinate islet-wide Ca^{2+} dynamics
- Functional subpopulations have been described in human beta cells and their distribution is altered in type 2 diabetes

What is the key question?

- Does NNAT mark a discrete subpopulation of functional beta cells, and which epigenetic pathways coordinate its formation and maintenance?

What are the new findings?

- A subpopulation of $NNAT^+$ beta cells is established prior to the first week of postnatal life in mice via de novo DNA methylation at the *Nnat* promoter
- $NNAT^+$ beta cells are transcriptionally highly differentiated and appear to be functionally specialised for insulin production, possibly corresponding to recently described 'β_{HI}' and '$CD63^{hi}$' beta cells. NNAT is expressed in a subset of beta cells across the human islet, and its deficiency in human beta cells diminishes glucose-stimulated insulin secretion
- $NNAT^+$ cells are likelier to belong to the population of 'follower' cells, rather than 'hub' cells, consistent with a role in insulin production rather than glucose detection

How might this impact on clinical practice in the foreseeable future?

- Epigenome-modifying compounds may provide a way of enhancing beta cell function and the ensemble behaviour of the islet to stimulate insulin secretion

methylation at this locus may contribute to a loss of beta cell hierarchy and connectivity, potentially contributing to defective insulin secretion in some forms of diabetes.

Data availability The mass spectrometry proteomics data have been deposited to the ProteomeXchange Consortium via the PRIDE partner repository with the dataset identifier PXD048465.

Keywords Beta cell development · Ca^{2+} · Connectivity · CpG methylation · Heterogeneity · Identity · Imprinted genes · Insulin · Islet · Neuronatin · Type 2 diabetes

Abbreviations

DMR	Differentially methylated region
DNMT3A	DNA methyltransferase 3 alpha
E	Embryonic day
eGFP	Enhanced GFP
ER	Endoplasmic reticulum
ETC	Electron transport chain
FDR	False discovery rate
GSEA	Gene set enrichment analysis
GSIS	Glucose-stimulated insulin secretion
HTRF	Homogeneous time-resolved fluorescence
NA	Numerical aperture
NNAT	Neuronatin
P	Postnatal day
RIP	Rat insulin promoter
scRNA-seq	Single-cell RNA-seq
shRNA	Short hairpin RNA
SPC	Signal peptidase complex
TOM20	Translocase of outer mitochondrial membrane 20
UCN3	Urocortin 3

Introduction

Insulin-producing beta cells are central to the modulation of glucose homeostasis, and their impaired function, loss of identity or lowered numbers result in type 2 diabetes [1].

Previous studies have provided an understanding of the transcriptional machinery that orchestrates beta cell development from early pancreatic and endocrine precursors [2]. To bolster these transcriptional programmes in vivo, chronic regulation via the epigenome appears to step in to maintain beta cell identity in the long term [3–7].

Early reports [8, 9], and more recent studies based on single-cell transcriptomic profiling [10–12], electrophysiology [13] and functional imaging [14–17], have demonstrated functional heterogeneity amongst individual beta cells (reviewed in [18]). Identified subpopulations have been associated with known markers or maturation states (*Flattop*/*Cfap126* [16], polysialyated-neural cell adhesion molecule [PSA-NCAM] [19], CD81 [20], CD24 [7, 21], tyrosine hydroxylase [TH] [6], neuropeptide Y (NPY) [22], CD63 [23]), are 'virgin' beta cells [24] or are defined by their roles in coordinating islet-wide Ca^{2+} dynamics (e.g. 'hubs' [14], 'leaders' [15, 25] and 'first responders' [26]). Furthermore, loss of beta cell heterogeneity or intercellular connectivity may contribute to the development of type 2 diabetes [14, 15, 27]. Importantly, functional subpopulations have also been demonstrated in human beta cells [11, 12, 28], and the distribution of antigenically defined sub-groups (based on CD9 and ST8 α-*N*-acetylneuraminide α-2,8-sialyltransferase [ST8SIA1] positivity) is altered in type 2 diabetes [10]. The features underlying beta cell heterogeneity include pathways governing glucose sensing and metabolism [14–16], insulin content and secretory competence [5, 13, 24, 29, 30], and cilia activity and localisation within the islet [25]. Recently, two discrete populations of '$CD63^{hi}$' and '$CD63^{lo}$' cells have been described [23], with '$CD63^{hi}$' cells enriched for CD63 and for insulin content and glucose-stimulated insulin secretion (GSIS). Epigenomically defined (by histone methylation, H3K27me3) CD24-positive 'β_{HI}' beta cells with enhanced insulin content and GSIS [7] may partly overlap the '$CD63^{hi}$' population [23].

Imprinted genes are expressed from a single allele in a parent-of-origin-specific manner and their expression is also controlled via epigenetic modifications, notably DNA methylation. Imprinted genes often play key physiological roles, particularly in early (fetal and postnatal) growth and development, controlling a wide range of cellular processes. Thus, human imprinting disorders involving altered expression from specific imprinted loci are associated with severe childhood developmental and metabolic complications (reviewed in [31]).

Imprinted genes play key functional roles in pancreatic beta cells by modulating insulin secretory machinery or beta cell mass [32]. Correspondingly, imprinted gene expression is dysregulated both in beta cells with diminished GSIS and in pancreatic islets from individuals with type 2 diabetes, and single nucleotide polymorphisms (SNPs) at imprinted loci are associated with type 2 diabetes risk [18]. Monoallelic expression of imprinted genes is maintained transgenerationally by differential methylation between parental alleles at imprinted loci in the germline [33], with additional 'somatic' or 'secondary' differentially methylated regions (DMRs) also established post fertilisation [34].

We have previously shown [35] that the paternally expressed, imprinted gene *Nnat* (encoding neuronatin [NNAT]) is nutrient-regulated in pancreatic beta cells, and controls insulin content and GSIS by modulating early insulin precursor processing at the signal peptidase complex (SPC) [35]. At extra-pancreatic sites, changes in *Nnat* expression also modulate appetite and metabolism [36–38]. Here, we explore the possibility that differential methylation of the *Nnat* gene contributes to the functional heterogeneity of embryonic and adult pancreatic beta cells.

Methods

For details, please refer to electronic supplementary material (ESM) Methods.

Bioinformatic clustering analysis Single-cell RNA-seq (scRNA-seq) embryonic and adult islet datasets [5, 39–42] were assessed for hypervariability of gene expression and unbiased clustering using the scran v1.28.2 (https://bioconductor.org/packages/release/bioc/html/scran.html) and RaceID v0.3.0 (https://cran.r-project.org/web/packages/RaceID/index.html) packages, respectively, as described in the ESM Methods.

Pseudo-time analysis scRNA-seq datasets [39] were processed with Seurat v4.3 and clustered and processed for pseudo-time analysis, followed by integration with a dataset from adult mouse islets [41, 42], according to the ESM Methods.

Study approval All animal procedures were in accordance with the UK Animals (Scientific Procedures) Act 1986 and approved by the UK Home Office (Project licence (PPL) number: PP4712156). All animal studies have been approved by the Imperial College Animal Welfare and Ethical Review Body.

Animal models Transgenic mouse lines expressing *Cre* recombinase under the control of the rat insulin promoter (RIP) [43] and with a tdTomato reporter downstream of a stop codon flanked by *loxP* sites [44] have been described previously. Mice with *Nnat*-driven enhanced GFP (eGFP) expression were purchased from the Mutant Mouse Resource and Research Centre (MMRRC, USA) repository [Tg(*Nnat*-EGFP)EA106Gsat/Mmucd, stock no. 010611-UCD]. Mice with global deletion of *Nnat* [35] and conditional *Dnmt3a* null mice generated by crossing to *Pdx1-Cre* are described in the ESM Methods. *db/db* and control C57BLKS/J mice on the BKS background were obtained from The Jackson Laboratory, USA (JAX 000642 and JAX 000662, respectively).

Primary islet isolation and FACS To isolate primary islets, the pancreas was inflated with Liberase TM (Roche, UK), digested at 37°C and purified using a Histopaque 1119/1083/1077 gradient (Sigma-Aldrich, UK), and islets were hand-picked. For FACS-based experiments, cells from purified islets were isolated using Accutase (Sigma-Aldrich) and sorted using a FACSAria III flow cytometer (BD Biosciences, UK), as detailed in the ESM Methods. Total insulin content was assessed using ultra-sensitive insulin homogeneous time-resolved fluorescence (HTRF) assay kits (Cisbio, France).

Intracellular calcium imaging Pancreatic islets from reporter mice expressing *Nnat*-eGFP were isolated as above, with Ca^{2+} imaging of whole islets performed after loading the cytosol with 2 μmol/l Cal-590 AM (Stratech, UK). Images were captured on an Axiovert microscope (Zeiss, Germany) equipped with a ×10, 0.3–0.5 numerical aperture (NA) objective and a ImagEM camera (Hamamatsu, Japan) coupled to a Nipkow spinning-disk head (CSU-10, Yokogawa, Japan) and illuminated at 490 nm or 530 nm.

For experiments involving global *Nnat* null mice [35], islets were incubated with 4.5 μmol/l Cal-520 AM (Stratech), and imaging was performed on a Nikon (Japan) Eclipse Ti microscope equipped with a ×40/1.2 NA oil objective and an ibidi heating system. Cal-520 AM was excited with a 491 nm laser line and emitted light filtered at 525/50 nm. Images were acquired with an ORCA-Flash 4.0 camera (Hamamatsu) and Metamorph software (Molecular Devices). Pearson-based connectivity and correlation analyses in an imaged islet were performed with Ca^{2+} signals smoothed, binarised and analysed as described in the ESM Methods.

Histological techniques and immunofluorescence Dissected tissues were fixed, cryoprotected and embedded in optimal cutting temperature (OCT) and stored at −80°C. Sections (10 μm) were cut using a CM1950 Cryostat (Leica, Germany) and immunostained using primary and secondary antibodies (listed in the ESM Methods), and imaged using a TCS SP5 confocal microscope (Leica). Immunostaining of paraffin-embedded pancreas from mice with beta cell-selective deletion of *Dnmt3a* was performed according to references [6, 22] as described in the ESM Methods. Human pancreases were processed, immunostained and imaged as described in the ESM Methods with the approval of the Ethics Committee of the University of Pisa, upon written consent of donors' next-of-kin.

Cell culture, RNA silencing and GSIS Human EndoC-βH1 and rat INS1E beta cells were cultured as previously described [35] and incubated with lentiviruses expressing an *NNAT*-targeting short hairpin RNA (shRNA; Sigma-Aldrich) or Silencer Select siRNAs (Ambion, USA), respectively, as described in the ESM Methods. GSIS assays were performed using ultra-sensitive insulin HTRF assay kits (Cisbio) for insulin quantification.

Immunoprecipitation and mass spectrometry Cells were processed for immunoprecipitation and incubated with antibodies against NNAT (ab27266, Abcam, UK, 1:500) prior to mass spectrometry analysis [35] as described in the ESM Methods.

Western immunoblotting, RT-PCR, RNA-seq For western blotting, EndoC-βH1 cells were processed as previously described [35] using primary antibodies against NNAT (ab27266, Abcam, 1:2000) and β-tubulin (clone 9F3, stock no. 2128, Cell Signaling, USA, 1:5000). For RT-PCR, mRNA was purified using Allprep or RNeasy kits (both Qiagen, Germany) and reverse transcribed, and cDNA was assessed by quantitative RT-PCR using Taqman reagents (all Life Technologies, USA) on a QuantStudio 7 Real Time PCR cycler.

For RNA-seq, RNA from FACS-purified cells was quantified and assessed for integrity using a Bioanalyzer 2100 and an RNA 6000 Pico assay (Agilent Technologies). RNA was processed using a NEBNext Ultra II Directional RNA Library Prep Kit for Illumina paired with a Poly(A) mRNA magnetic isolation module and AMPure XP SPRIselect beads (Beckman Coulter, UK). Libraries were sequenced using a NextSeq 500 High Output sequencer (Illumina, USA), with 2×75 bp length at 50 million reads per sample. Further details can be found in the ESM Methods.

Bisulphite sequencing Genomic DNA was extracted from FACS-purified cells using Allprep DNA/RNA/protein mini kits from Qiagen. Bisulphite sequencing experiments were performed using an EZ DNA Methylation-Gold kit from Zymo Research, USA, an EpiTaq hot start kit (TaKaRa Bio, Japan) and a CloneJET PCR cloning kit (Life Technologies), with DNA purified using a Wizard SV 96 plasmid system (Promega, USA) before Sanger sequencing (Genewiz, now Azenta Life Sciences, UK), and then analysed using bisulphite sequencing DNA methylation analysis (BISMA) software.

Statistical analysis Data are shown as mean±SEM in all figure panels. Data were assessed using GraphPad Prism 9.0, with <5% error probability considered significant (i.e. $p<0.05$). Further statistical information, such as n numbers and p values, are provided in the figure legends.

Results

NNAT expression is heterogeneous across the islet and represents a highly differentiated beta cell subtype We have previously shown that *Nnat* is crucial for insulin storage and

GSIS in the mouse [35]. NNAT expression is diminished in rodent models of obesity and diabetes including the Zucker diabetic fatty (ZDF) rat model (85% decrease, p=0.0023, n=5 [45]) and obese *ob/ob* mice (ESM Fig. 1a). Pancreatic sections of *db/db* mice displayed a loss of NNAT immunoreactivity across islets, and a significant reduction of NNAT$^+$ beta cells (ESM Fig. 1b,c).

Reanalysis of published scRNA-seq datasets from primary mouse beta cells at embryonic (embryonic day 17.5 [E17.5]) [39, 40] and adult [5, 41, 42] stages identified *Nnat* as amongst the most highly variable genes between individual cells (ESM Table 1). Pseudo-time analysis of embryonic (E12.5 to E17.5) mouse beta cells [39] clearly demarcated the differentiation of beta cells through embryonic cell

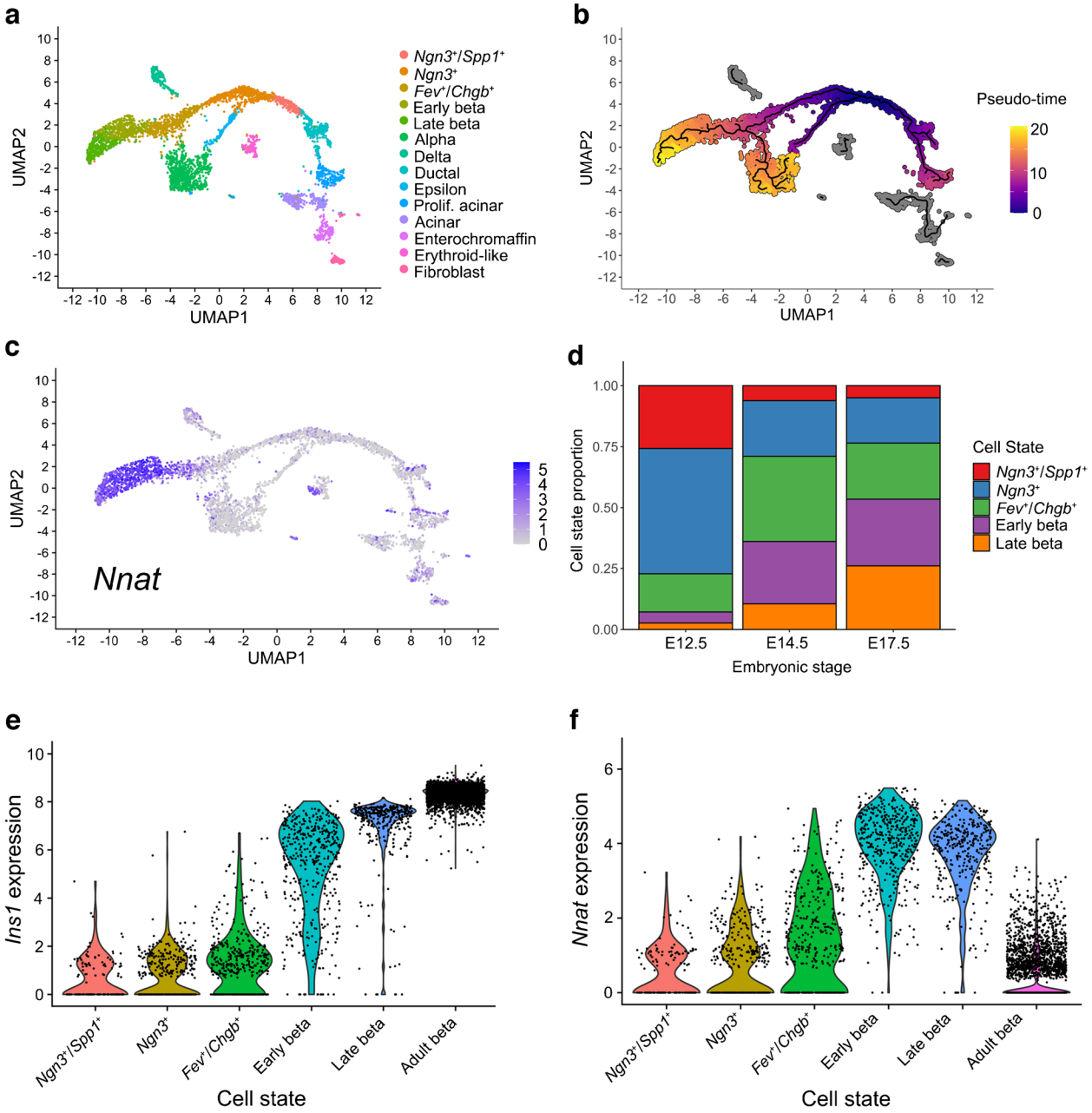

Fig. 1 *Nnat* expression is a marker for late-stage beta cell differentiation during islet development. (**a**–**c**) UMAP projection of scRNA-seq data from embryonic mouse islets (E12.5–E17.5), with cells labelled by their cellular state (**a**), pseudo-time (scale bar represents abstract unit of time) (**b**) and corresponding *Nnat* expression (log-normalised expression level) (**c**). (**d**) Changes in the distribution of beta cell precursors from E12.5 to E17.5. (**e**, **f**) Violin plots showing the fluctuations in *Ins1* (**e**) and *Nnat* (**f**) expression (both log-normalised expression level) from E12.5 to adulthood in the beta cell development trajectory. Prolif., proliferating; UMAP, uniform manifold approximation and projection

states, with late embryonic (E17.5) beta cells overlapping with high levels of *Nnat* expression (Fig. 1a–c, ESM Figs 2a–f, 3a–k). Analysis of the proportions of different beta cell progenitors revealed that *Nnat*$^+$ cells become more prominent at later stages of development (Fig. 1d). Integrating cells from the embryonic beta cell trajectory with adult beta cells [41, 42] allowed us to evaluate the progressive change in beta cell markers and *Nnat* expression from development to maturity (Fig. 1e,f, ESM Fig. 4a–i), and revealed large increases in *Ins1* expression alongside *Nnat* downregulation in most beta cells. Nevertheless, a considerable number of adult beta cells (with high expression of *Ins1*/*Ins2*) also expressed *Nnat* (Fig. 1f). Thus, *Nnat* appears to mark late-stage beta cell differentiation, peaking in expression around E17.5 and then gradually being downregulated across most beta cells in adulthood.

In light of the abundance of *Nnat*$^+$ beta cells during late embryogenesis, we further evaluated the E17.5 dataset [39] and again identified two beta cell populations with distinct levels of *Nnat* expression (Fig. 2a–c, ESM Fig. 5a–f). Embryonic *Nnat*$^+$ beta cells were enriched for *Ins1*, *Ins2*, *Nkx6.1*, *Pdx1*, *Ucn3*, *Slc2a2*, *Iapp*, *Ero1b*, *G6pc2*, *Dlk1* and *Npy* expression compared with *Nnat*$^-$ beta cells which had higher *Neurog3*, *Pax4*, *Gcg*, *Arx* and *Ghrl* expression, indicating that the *Nnat*$^+$ beta cells were more fully differentiated (Fig. 2d, ESM Table 2). *Nnat*$^+$ beta cells were also de-enriched for *Cd24a* (Fig. 2d, ESM Table 2). Gene set enrichment analysis (GSEA) revealed upregulation of processes related to protein synthesis, transport from endoplasmic reticulum (ER), ER stress, as well as oxidative phosphorylation and carbohydrate metabolism, with downregulated processes including mRNA processing, splicing and histone methylation (Fig. 2e). Indeed, a separate cell clustering analysis [46] identified *Nnat* as a highly differentially expressed gene between two beta cell clusters at both the late embryonic [39, 40] and adult [5] stages (ESM Figs 6a–h, 7a–g, ESM Table 3).

We confirmed some of these findings at the protein level using immunofluorescence in postnatal and adult mice (Fig. 3a,b). We noted that NNAT protein expression is highly dynamic in beta cells across the mouse islet throughout the postnatal stage, transitioning from expression throughout the majority (90.4±3.2%, n=15 mice) of beta cells at late

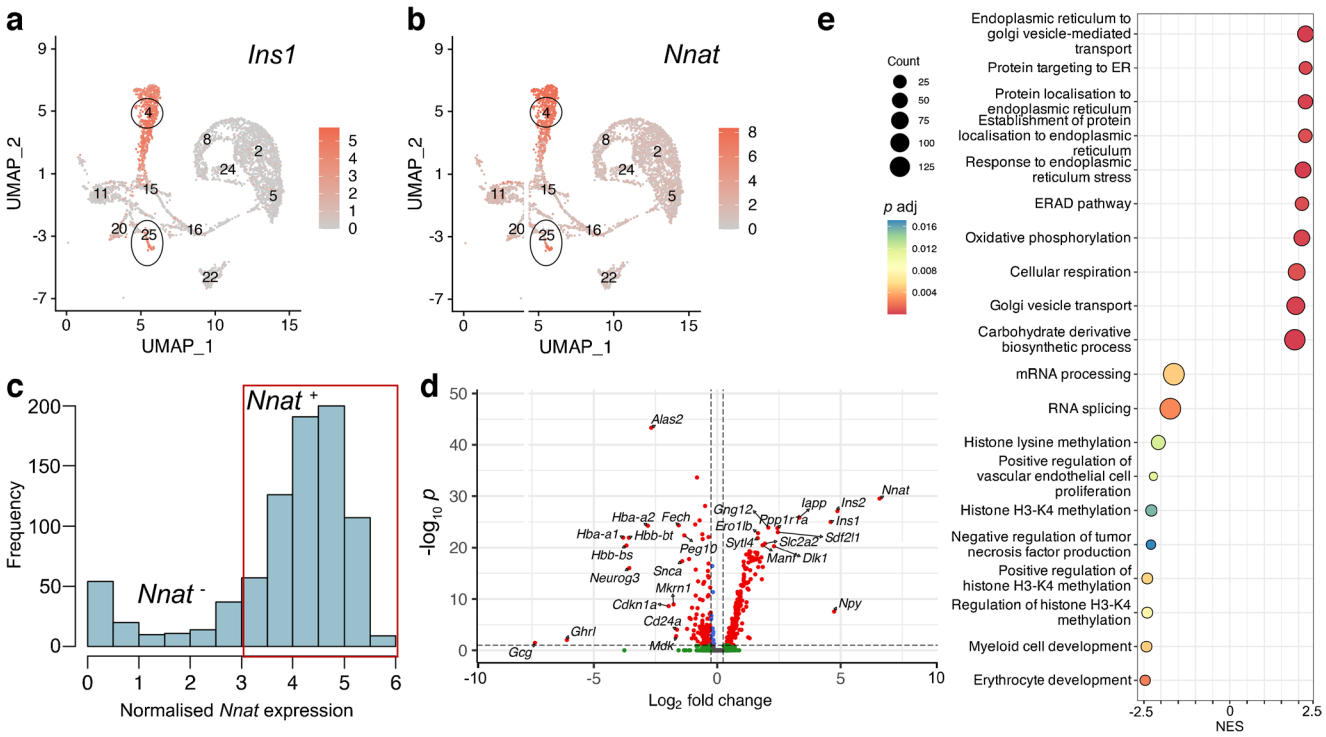

Fig. 2 Transcriptomic analyses of islet cells at E17.5 reveal *Nnat*$^+$ cells to be a more differentiated beta cell subcluster. (**a**, **b**) Islet cells plotted in the UMAP space and coloured by *Ins1* (**a**) and *Nnat* (**b**) expression, respectively. Individual cellular clusters are labelled. Beta cell clusters are highlighted with black circles. (**c**) Distribution of *Nnat* expression among beta cell clusters, along with the expression range used in defining *Nnat*$^+$ beta cells (highlighted by the red rectangle). (**d**) Volcano plot showing the $\log_2$ fold change in gene expression between *Nnat*$^+$ and *Nnat*$^-$ beta cells against FDR-corrected p values. Genes with FDR<0.1 are coloured red. Top ten upregulated and downregulated genes are labelled by gene name. (**e**) GSEA of differentially expressed genes between *Nnat*$^+$ and *Nnat*$^-$ beta cells (using gene ontology-biological process [GO-BP] terms), showing the top ten upregulated and downregulated processes. The normalised enrichment score (NES) is plotted along the x-axis. Circle diameters are proportional to the number of genes in each process, with the colours defining statistical significance. UMAP, uniform manifold approximation and projection

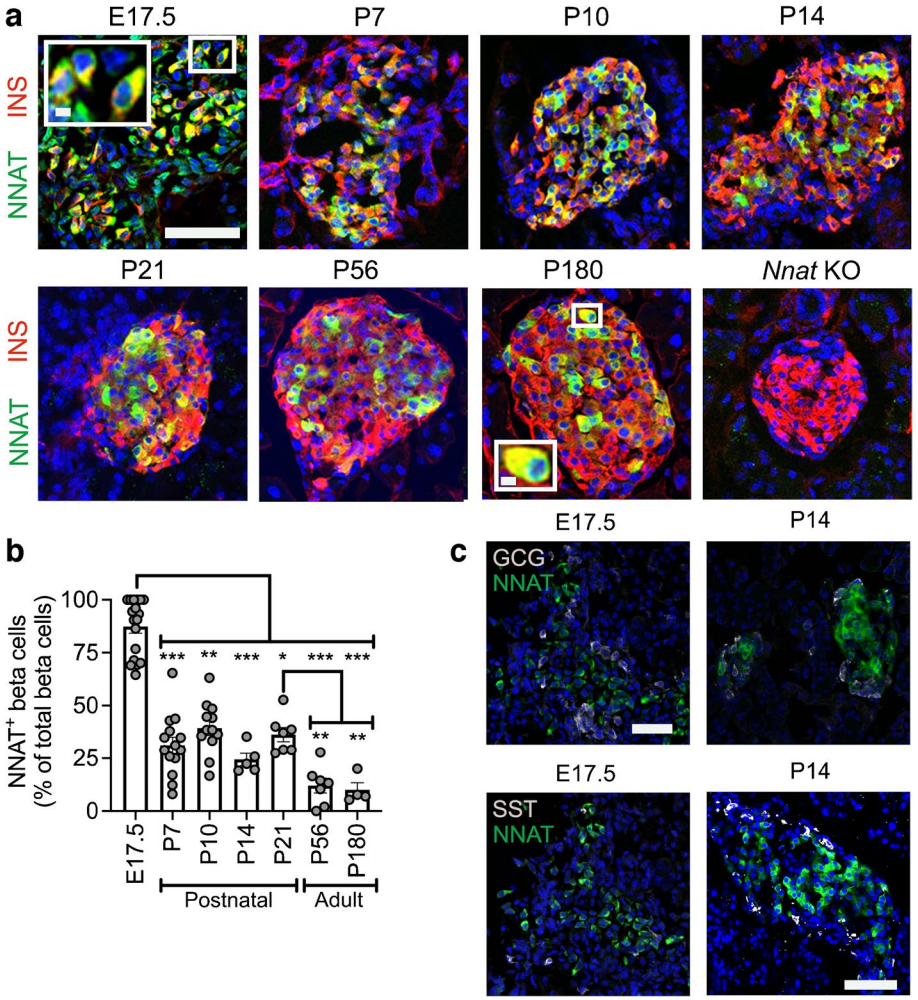

Fig. 3 A subpopulation of NNAT$^+$ beta cells develops during the early postnatal period in mice. (**a**) Representative confocal microscopy of pancreatic cryosections from wild-type mice on a C57BL/6J background of developmental stages from E17.5 through the postnatal period into adulthood. Sections were immunostained with antibodies against endogenous NNAT (green) and insulin (INS, red). Nuclei are visualised with DAPI and sections from P56 mice with constituent deletion of *Nnat* were used as an immunostaining control. Scale bar, 100 μm (inset, 10 μm). (**b**) Quantification of NNAT$^+$ beta cells from images shown in (**a**), expressed as NNAT/INS co-positive cells as a percentage of total INS-positive cells (n=4–15 mice per timepoint, Kruskal–Wallis test with Dunn's multiple comparisons). (**c**) Representative confocal microscopy of pancreatic cryosections as in (**a**) from E17.5 and P14 mice (n=18 and n=5 mice, respectively) immunostained with antibodies against endogenous NNAT (green) and GCG or SST (both grey). Scale bar, 100 μm. Representative images from three independent experiments and breeding pairs. *p<0.05, **p<0.01, ***p<0.001. GCG, glucagon; KO, knockout; SST, somatostatin

embryogenesis to a subset (24.4±3.0%, n=5 mice) of beta cells by postnatal day 14 (P14) (Fig. 3a,b). NNAT$^+$ beta cells persisted throughout the islet into adulthood (Fig. 3a,b). NNAT expression was not apparent in other mouse islet cell types, including alpha and delta cells, at P14. However, NNAT expression was detectable in a small number of alpha and delta cells at E17.5 (Fig. 3c).

NNAT immunoreactivity is detected in a subset of beta cells in human islets and NNAT deficiency in human beta cells blunts GSIS While the role of NNAT has previously been examined in mouse beta cells [35], no data currently exist for human beta cells. We therefore next compared the functionality of human NNAT$^+$ and NNAT$^-$ beta cells. Transient silencing of *NNAT* in human EndoC-βH1 beta cells completely abrogated glucose-stimulated insulin release (Fig. 4a–c). As in mouse beta cells [35], NNAT interacted in cellulo with subunits of the SPC, SEC11A, SPCS1, SPCS2 and SPCS3 (ESM Fig. 8a), likely via SPCS1 (ESM Fig. 8b).

Heterogeneous expression of NNAT in human islet cells was also observed in whole pancreatic sections from multiple donors. Thus, NNAT was expressed in a subset of beta cells in both younger (15.6±0.9 years, 15.0±4.0%, n=5) and older (71.0±3.9 years, 17.7±2.1%, n= 4) donors (Fig. 4d,e, ESM

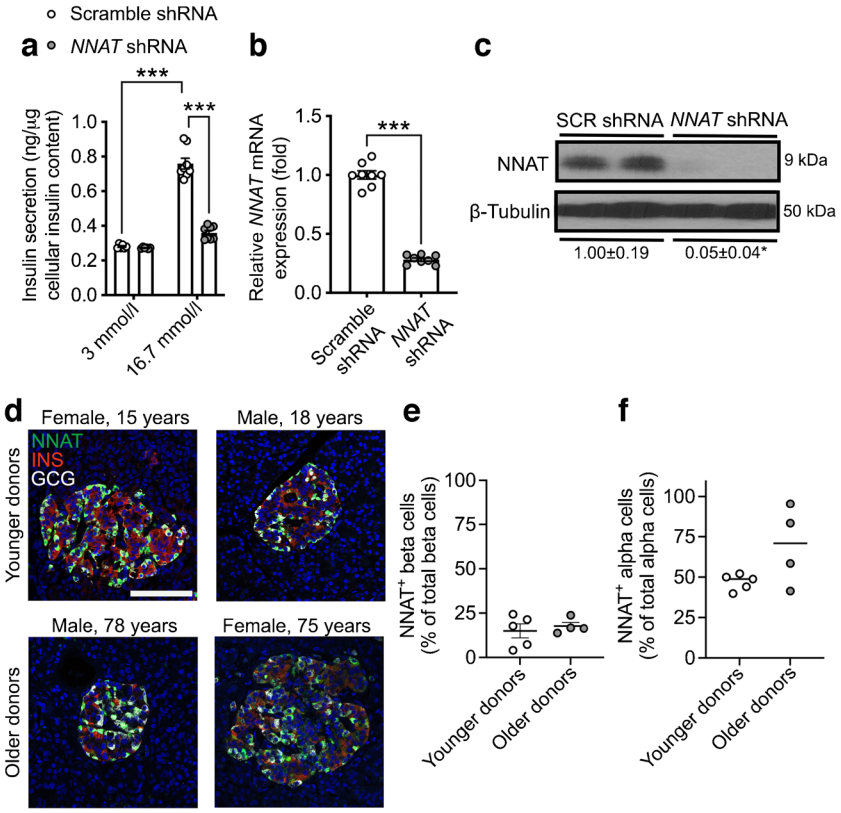

Fig. 4 NNAT is expressed in a subset of human beta cells and NNAT deficiency in human beta cells reduces insulin secretion. (**a**) GSIS analysis at low (3 mmol/l) and high (16.7 mmol/l) glucose in human EndoC-βH1 beta cells following 72 h of lentiviral-mediated shRNA knockdown of NNAT with data expressed as insulin secreted into culture media as a percentage of total cellular insulin content (n=8 independent cultures per group, two-way ANOVA with Sidak's multiple corrections test). (**b**, **c**) RT-PCR (n=8, unpaired Student's t test) and western blot (n=4, Mann–Whitney U test) analysis of NNAT expression in EndoC-βH1 beta cells after transient *NNAT* silencing as in (**a**). (**c**) Western blotting analysis of NNAT protein levels shown via a representative blot of two independent experiments. β-Tubulin was used as a loading control. Mean values for band intensities in multiple experiments quantified by densitometry are shown below the panel, expressed relative to scramble (SCR) shRNA controls. (**d**) Representative confocal microscopy of human pancreatic cryosections from younger (15.6±0.9 years, n=5) and older (71.0±3.9 years, n=4) donors. Sections were immunostained with antibodies against endogenous NNAT (green), insulin (INS, red) and glucagon (GCG, grey). Donor sex and age are indicated in the text. Nuclei are visualised with DAPI. Scale bar, 100 µm. (**e**, **f**) Quantification of NNAT$^+$ beta (**e**) and alpha (**f**) cells from images shown in (**d**), expressed as NNAT/INS or NNAT/GCG co-positive cells as a percentage of total INS-positive or GCG-positive cells. *p<0.05, ***p<0.001

Fig. 9a, ESM Table 4, ESM Human Islet Checklist). Interestingly, NNAT was also expressed in a large fraction of human alpha cells (but not in delta cells, Fig. 4d,f, ESM Fig. 9b) in both younger (47.0±2.2%) and older donors (69.6±12.2%).

Heterogeneous NNAT expression in beta cells during postnatal development is associated with altered CpG methylation To extend the findings above using an orthogonal approach, and to facilitate subsequent functional studies, we utilised a Bacterial Artificial Chromosome (BAC) reporter mouse line expressing eGFP under the control of the *Nnat* promoter and upstream enhancers (ESM Results, ESM Fig. 10a–e). Aligning with studies of the endogenous gene (Figs 1, 2, 3 and 4), adult reporter mice expressed eGFP in a subpopulation (~15% of total) of beta cells (Fig. 5a).

To isolate and purify beta cells based on NNAT levels, we crossed *Nnat*-eGFP reporter mice to animals expressing *Cre* recombinase under the RIP [43] and to transgenic mice expressing a tdTomato reporter downstream of a *lox*P-flanked stop codon [44]. Dispersion of primary adult islets into single cells, and subsequent FACS analysis, verified the presence of NNAT$^+$ and NNAT$^-$ beta cells, with the NNAT$^+$ fraction composing 15.3±1.8% (n=8 mice) of the total beta cell compartment (Fig. 5b,c, ESM Figs 11a,b, 12a–f). Collection of FACS-purified NNAT$^+$ and NNAT$^-$ beta cells and subsequent bisulphite sequencing analysis revealed that CpG methylation at the gametic DMR (known to control monoallelic *Nnat* expression; Introduction) was unchanged (ESM Fig. 11c–e). Nevertheless, CpG methylation at the *Nnat* promoter was significantly altered across this genomic region,

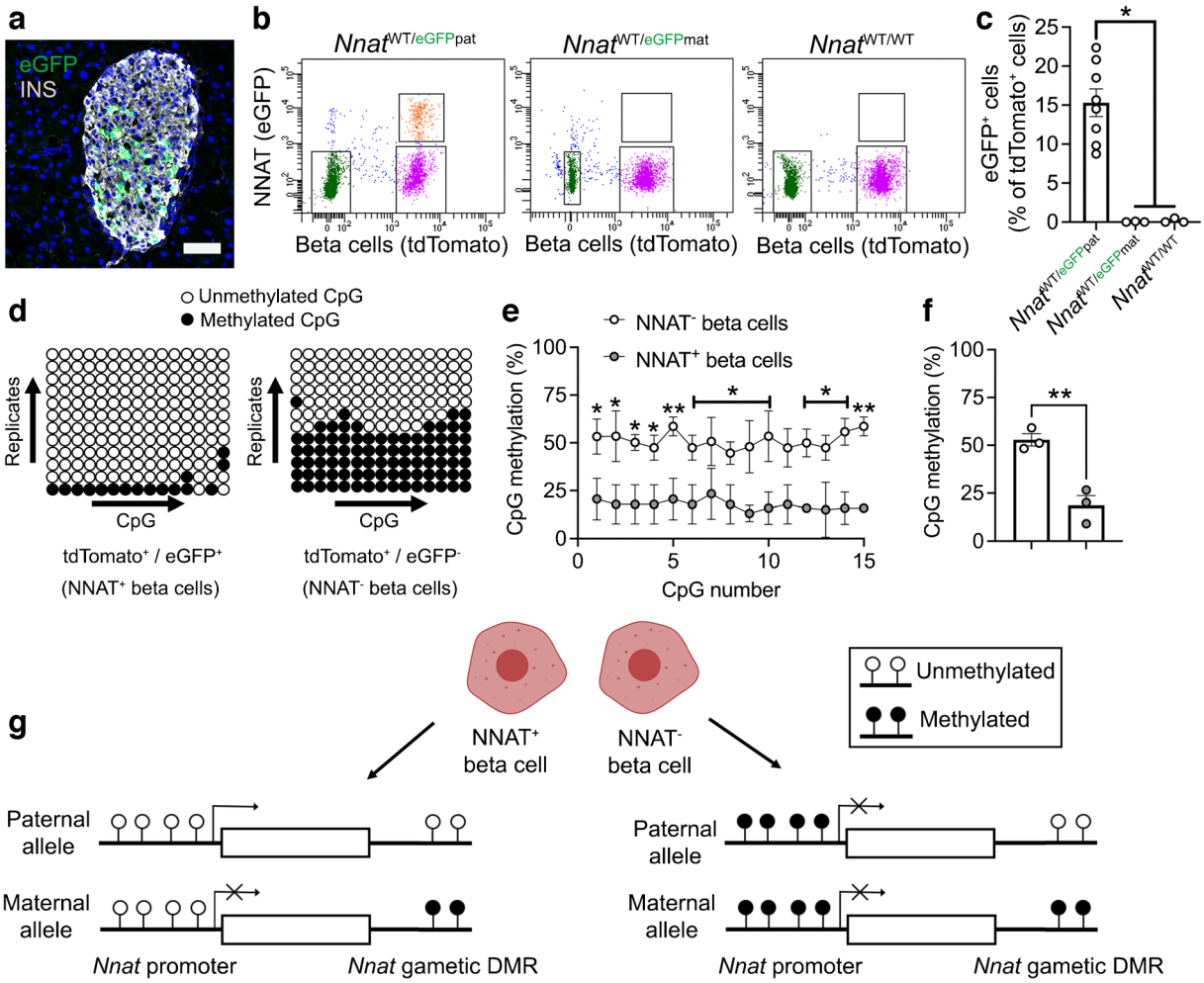

Fig. 5 Beta cell heterogeneity of NNAT expression is associated with changes in CpG methylation at the *Nnat* promoter. (**a**) Representative confocal microscopy of pancreatic cryosections from P56 mice with *Nnat*-driven eGFP expression from the paternal allele (*Nnat*$^{WT/eGFPpat}$) (n=7 mice). Sections were immunostained with antibodies against eGFP (green) and insulin (INS, grey). Nuclei are visualised with DAPI. Scale bar, 50 µm. (**b**) FACS separation of dispersed primary islet cells from reporter mice with insulin-driven expression of tdTomato (to label beta cells) and *Nnat*-driven eGFP expression from the paternal (*Nnat*$^{WT/eGFPpat}$) or maternal (*Nnat*$^{WT/eGFPmat}$) allele or wild-type (*Nnat*$^{WT/WT}$) at this locus (representative FACS plot of the dispersed islet preparation from a single mouse shown) (n=8, 3 and 3 mice per genotype, respectively, Kruskal–Wallis test with Dunn's multiple comparisons). (**c**) Quantification of data in (**b**) expressed as percentage of eGFP/tdTomato co-positive primary islet cells. (**d**) Representative bisulphite analysis of CpG methylation at the *Nnat* promoter in FACS-purified islet cell populations from (**b**) (n=3 *Nnat*$^{WT/eGFPpat}$ mice with paternally expressed *Nnat*-driven eGFP, $n\geq12$ clones each). Closed circles, methylated CpG; open circles, unmethylated CpG. (**e**, **f**) Quantification of data in (**d**) expressed as percentage CpG methylation across the *Nnat* promoter at individual CpGs (**e**) and across the entire *Nnat* promoter (**f**) (both paired Student's t test). (**g**) Schematic summarising level of CpG methylation at the *Nnat* promoter and gametic DMR in NNAT$^+$ vs NNAT$^-$ beta cells (created with BioRender.com). Representative image in (**a**) and bisulphite analyses in (**d**) used experimental mice from three independent experiments and breeding pairs. *p<0.05, **p<0.01

with minimal CpG methylation observed in NNAT$^+$ beta cells (Fig. 5d–f).

Recent whole-genome methylation analysis in mouse germ cells has revealed that the *Nnat* promoter region is unmethylated in sperm, and this was confirmed by targeted bisulphite sequencing analysis (ESM Fig. 11f–h), whereas it is fully methylated in oocytes [47]. Thus, the 'classical' imprinting of *Nnat* is unaltered between beta cell subtypes with near binary ('on/off') expression of NNAT. However, and overlaying this control, a second DMR at the *Nnat* promoter within the non-imprinted allele dictates beta cell subtype specificity of expression (Fig. 5g).

The de novo DNA methyltransferase DNMT3A establishes NNAT beta cell subtype specificity To ask whether this apparent transition in *Nnat* expression in the early postnatal period is driven by de novo CpG methylation, we assessed endogenous NNAT beta cell immunoreactivity in postnatal

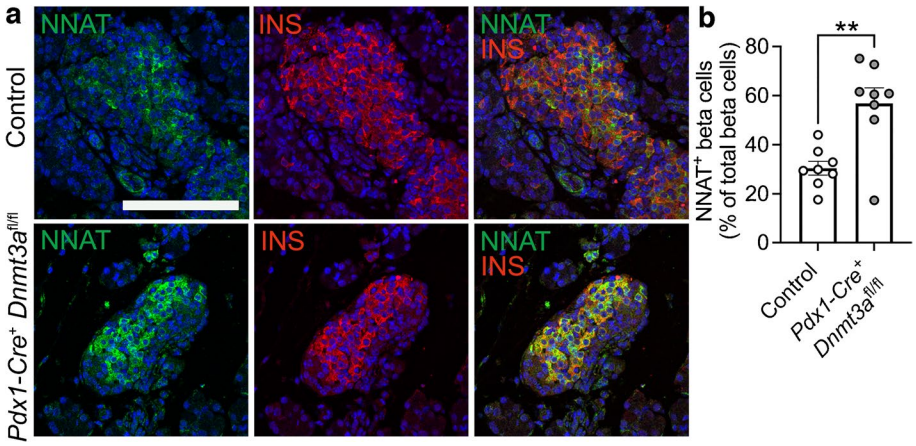

Fig. 6 Postnatal restriction of NNAT in a subset of beta cells is at least partially driven by the de novo methyltransferase DNMT3A. (**a**) Representative confocal microscopy of pancreatic cryosections from mice with conditional deletion of DNMT3A under the control of the *Pdx1* promoter (*Pdx1-Cre*$^{+}$ *Dnmt3a*$^{fl/fl}$) vs control (*Pdx1-Cre*$^{-}$ *Dnmt3a*$^{fl/fl}$) mice at P6. Sections were immunostained with antibodies against endogenous NNAT (green) and insulin (INS, red). (**b**) Quantification of NNAT^{+} beta cells from images shown in (**a**), expressed as NNAT/INS co-positive cells as a percentage of total INS-positive cells. Scale bar, 50 μm (n=8 mice per genotype, unpaired Student's t test, $^{**}p<0.01$). Nuclei are visualised with DAPI

mice conditionally deleted for the methyltransferase DNA methyltransferase 3 alpha (DNMT3A) at the pancreatic progenitor stage (using *Pdx1-Cre*) [6]. NNAT staining in control mice at P6 demonstrated expression in a subpopulation of beta cells, whereas deletion of DNMT3A resulted in a loss of this heterogenous expression across the islet (Fig. 6a,b, ESM Fig. 13a). These findings demonstrate that de novo methylation is likely to drive NNAT restriction across the beta cell complement in the first few days of postnatal life.

NNAT^{+} and NNAT^{-} beta cells have distinct transcriptional signatures In contrast to the embryonic populations described above, RNA-seq revealed that FACS-sorted adult (8 weeks) NNAT^{+} and NNAT^{-} beta cells displayed high transcriptional overlap and were similar to each other when compared with non-beta endocrine cells (Fig. 7a). Major beta cell identity markers such as *Ins1*, *Ins2*, *Mafa*, *Slc2a2* (*Glut2*) and *Nkx6.1* were not differentially expressed (ESM Table 5).

Nevertheless, we identified 241 (1.8%) and 79 (0.6%) genes that were significantly down- and upregulated in NNAT^{+} vs NNAT^{-} beta cells, respectively (>2-fold, false discovery rate [FDR]<0.01). Differentially expressed genes included several markers of non-beta cell islet lineages (*Pyy*, *Ppy*, *Mafb*, *Sst*) that were lower in the NNAT^{+} beta cell fraction, genes linked with beta cell heterogeneity and plasticity (*Gpx3*, *Rbp4*), the beta cell immaturity marker *Cd81* [20] and the *Cd24a* antigen [21] (Fig. 7b). Interestingly, *Npy* was enriched in NNAT^{+} beta cells (ESM Table 5), consistent with our observations at late embryogenesis (E17.5, Fig. 2d). We did not observe any clear differences between NNAT^{+} and NNAT^{-} beta cells in the expression of other imprinted genes known to be functional in the beta cell (*Plagl1*/*ZAC*, *Dlk1*, *Rasgrf1*, *Cdkn1c*, *Grb10* and *Gtl2*/*MEG3*), nor changes in 'disallowed' genes whose expression is known to be restricted in mature functional beta cells (*Hk1*, *Mct1* [*Slc16a1*] and *Ldha*) [48] (ESM Table 5). Likewise, no differences were apparent in the levels of transcripts encoding proteins previously demonstrated by others to mark specific beta cell subpopulations, such as *Flattop*/*Cfap126* [16], *CD9* and *ST8SIA1* [10], *Cd63* [23], 'virgin' beta cells (via *Ucn3*) [24] or those differentially expressed in beta cells implicated in the control of Ca^{2+} dynamics ('hubs' [14], and 'leaders' [15, 26]).

GSEA did, however, reveal enrichment of pathways in NNAT^{+} beta cells including translation initiation, the electron transport chain (ETC), oxidative phosphorylation and signal recognition particle (SRP)-dependent co-translational protein targeting (Fig. 7c). Pathways involving genes associated with hepatocyte nuclear factor 1 alpha (HNF1A) and GLI-similar family zinc finger 3 (GLIS3) targets were reduced in the NNAT^{+} beta cell fraction (Fig. 7d). NNAT^{+} beta cells displayed higher levels of the late maturation marker urocortin 3 (UCN3) (Fig. 7e, 0.357±0.009 in NNAT^{+} vs 0.264±0.004 arbitrary units in NNAT^{-}, $^{**}p<0.01$, 290 NNAT^{+}/1876 NNAT^{-} beta cells from 13 islets/n=3 mice) and a small but significant increase in translocase of outer mitochondrial membrane 20 (TOM20) immunostaining, consistent with a higher mitochondrial volume or number (Fig. 7f–h). Furthermore, FACS-sorted primary NNAT^{+} beta cells had a significantly higher insulin content than NNAT^{-} cells (Fig. 7i).

The NNAT^{+} beta cell population shows impaired glucose-stimulated Ca^{2+} dynamics and is de-enriched for highly connected 'hub' cells To determine whether NNAT may influence beta

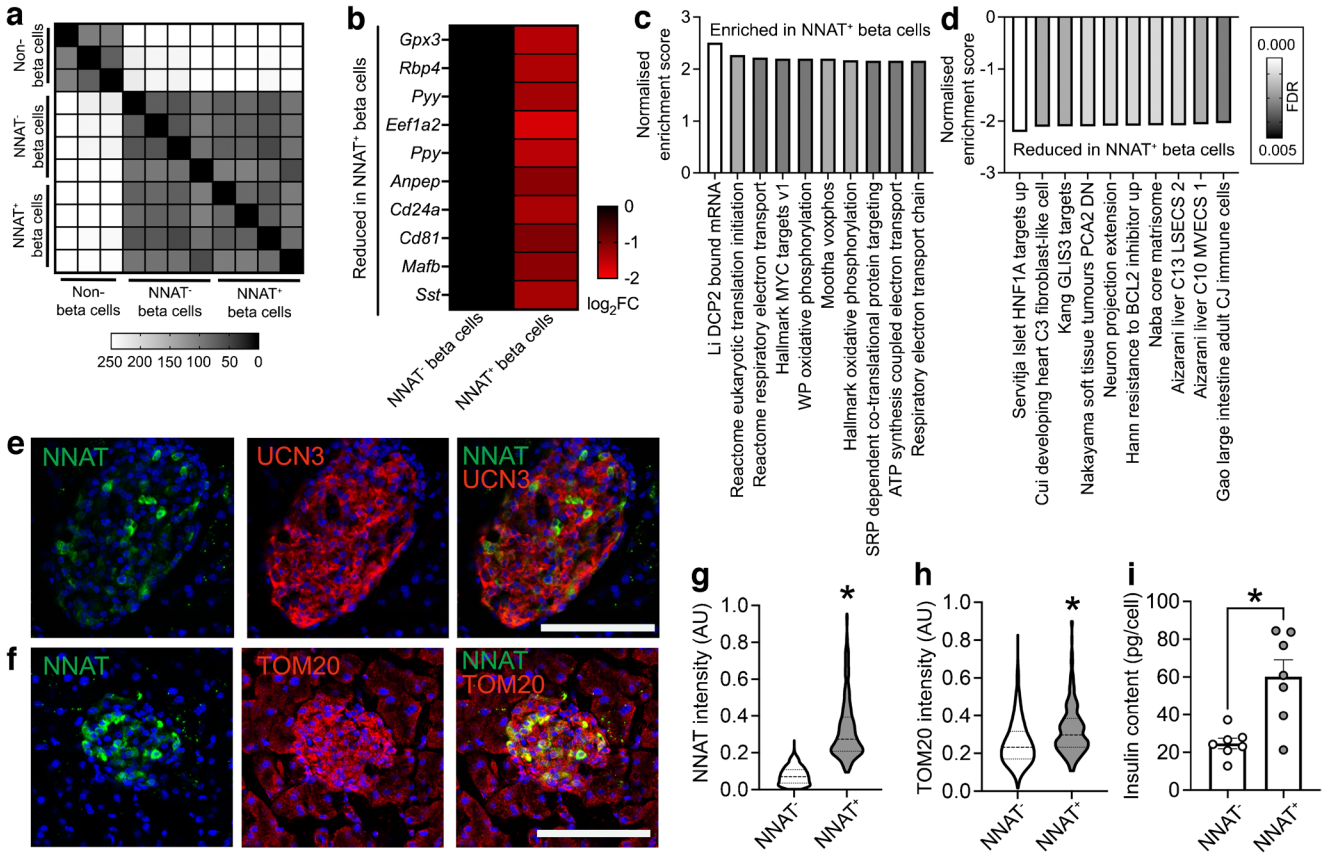

Fig. 7 NNAT$^+$ adult beta cells are transcriptionally distinct and have significantly higher insulin content. (**a**) Correlation matrix of differentially expressed genes between NNAT$^+$ and NNAT$^-$ beta cells as assessed by RNA-seq analysis (n=4 FACS-purified populations from individual mouse islet preparations). Scale bar (0–255) gives an integer provided to the R function where the darker colour corresponds to higher sample correlation. (**b**) Heatmap of the top ten most differentially expressed genes reduced in NNAT$^+$ beta cells compared with NNAT$^-$ beta cells. (**c**, **d**) GSEA showing categories significantly enriched (**c**) and reduced (**d**) in NNAT$^+$ (vs NNAT$^-$) beta cells. (**e**, **f**) Representative confocal microscopy of pancreatic cryosections from P56 (8-week-old) wild-type mice on a C57BL/6J background immunostained with antibodies against endogenous NNAT (green) and UCN3 (red, **e**) or TOM20 (red, **f**). Scale bar, 100 μm. Nuclei are visualised with DAPI. Representative images from three independent experiments and breeding pairs (**g**, **h**). Quantification of NNAT (**g**) and TOM20 (**h**) staining in NNAT$^-$ and NNAT$^+$ beta cells (INS$^+$) from images shown in (**f**), expressed as mean intensity of the NNAT or TOM20 channel (*p<0.05, paired Student's t test, 1329 NNAT$^-$ and 295 NNAT$^+$ beta cells from 15 islets, n=3 mice). (**i**) Insulin content assessed in NNAT$^+$ and NNAT$^-$ beta cells (*p<0.05, n=7 FACS-purified populations from individual mouse islet preparations, Wilcoxon matched-pairs signed rank test). AU, arbitrary units; FC, fold change

cell connectivity and membership of the 'hub' cell subgroup [14], we studied glucose-induced Ca^{2+} dynamics in *Nnat*-deficient (*Nnat*$^{+/-p}$) islets [35]. Ca^{2+} increases in response to high (11 mmol/l) glucose were significantly higher in *Nnat*$^{+/-p}$ than control islets, and while the mean Pearson's coefficient of correlation and proportion of highly connected 'hub' cells were not significantly different between *Nnat*-deficient and control islets (ESM Results, ESM Fig. 14a–d), wild-type 'hub' cells were significantly more connected than *Nnat*-deficient 'hub' cells (ESM Fig. 14e,f). Thus, NNAT is a marker of less well-connected cells.

We further explored this question using islets from *Nnat*-eGFP reporter mice, using the red-shifted calcium probe Cal-590 AM [49]. *Nnat*-GFP$^+$ and *Nnat*-GFP$^-$ cells responded similarly to challenge with high (11 mmol/l) glucose (Fig. 8a). Beta cell–beta cell connectivity (Fig. 8b) was not different between NNAT$^+$ and NNAT$^-$ populations and, considered across the whole population, the mean Pearson's coefficient of correlation was 0.87±0.01 (Fig. 8c).

Of all cells examined, 4.27% were NNAT$^-$ 'hub' cells (Ca^{2+} responses with at least 30% of all cells, Fig. 8d) connected to an mean of 39.0% of all beta cells (Fig. 8e,f). The fraction of these (1.15%, Fig. 8e) identified as NNAT$^+$ 'hub' cells had an mean of 38.3% coactivity with other cells (Fig. 8f). However, when considered within each individual islet, a significantly lower ratio of 'hubs' to 'followers' was observed in NNAT$^+$ vs NNAT$^-$ cells (Fig. 8g). Overlap with 'leader' cells [15, 25] was not explored in the absence of readily identifiable Ca^{2+} waves.

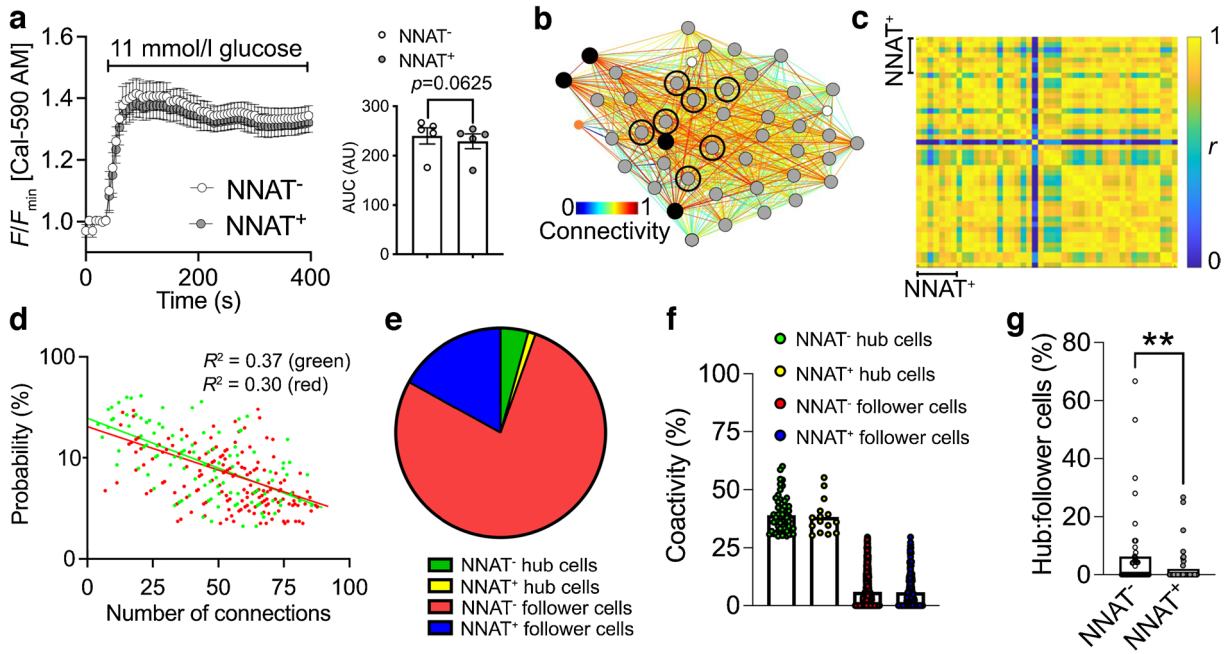

Fig. 8 NNAT$^+$ beta cells show altered glucose-induced Ca^{2+} dynamics and are de-enriched for highly connected 'hub' cells within individual islets. (**a**) Ca^{2+}-bound Cal-590 AM fluorescence in response to high glucose (11 mmol/l) in NNAT$^-$ and NNAT$^+$ cells from primary islets from *Nnat*$^{WT/eGFPpat}$ reporter mice expressed as normalised intensity over time (F/F_{min}) (n=61 islets total from five mice per genotype; quantification of AUC on the right, p=0.063, Wilcoxon matched-pairs signed rank test). (**b**) Representative Cartesian map of beta cells with colour-coded lines connecting cells according to the strength of coactivation (colour-coded R values from 0 to 1, blue to red). Beta cells are represented by differently coloured nodes depending on their coactivity with the other beta cells, where black nodes indicate coactivity with ≥80% of the remaining beta cells, while grey, white and orange nodes represent coactivity with ≥60%, ≥40% and <40%, respectively. Nodes circled with a solid black line indicate NNAT$^+$ cells. (**c**) Representative heatmaps depicting connectivity strength (r) of all cell pairs (colour-coded r values from 0 to 1, blue to yellow). (**d**) Log–log graphs of beta cell–beta cell connectivity distribution. NNAT$^+$ cells are represented by green circles while NNAT$^-$ cells are represented by red circles (45 islets total using primary islet preparations, each from an individual *Nnat*$^{WT/eGFPpat}$ reporter mouse). (**e**) Categorisation of beta cells based on data from (**d**). (**f**) Percentage coactivity of beta cells between all cells in identified 'hub' and 'follower' cells. (**g**) The proportion of cells designated as 'hub' vs 'follower' cells in both the NNAT$^-$ and NNAT$^+$ populations assessed in each of 45 islets (**p<0.01, Wilcoxon matched-pairs signed rank test). Analyses in panels (**a**–**g**) obtained from three independent experiments and three different breeding pairs of experimental mice. AU, arbitrary units

Discussion

We describe here a novel subgroup of beta cells characterised by transient methylation of a second DMR (but not the gametic DMR) in the *Nnat* locus. This is consistent with previous findings that methylation at gametic DMRs is thought to be relatively stable [50], whereas 'secondary' imprinting regions have been shown to be more sensitive to nutrient- or physiology-based changes [6, 51]. We have previously described the importance of *Nnat* for beta cell insulin content and secretion [35] and therefore hypothesise that NNAT$^+$ and NNAT$^-$ cells display differences in secretory function. Correspondingly, transcriptomic analysis of purified adult NNAT$^+$ and NNAT$^-$ beta cells demonstrated that the NNAT$^+$ fraction is enriched for functional pathways including translation initiation, ETC/oxidative phosphorylation pathways and co-translational protein ER membrane targeting.

Extending these studies to humans, NNAT deficiency in human EndoC-βH1 beta cells severely blunted GSIS, likely via inhibition of signal peptidase-mediated processing [35]. We show here that E17.5 *Nnat*$^+$ beta cells are enriched for expression of the SPC and translocon apparatus (*Spcs1*, *Spcs2*, *Sec11a*, *Sec11c*, *Sec61*) and that the SPC/NNAT interaction is via SPCS1, and likely the means through which NNAT influences cellular insulin content. Importantly, we demonstrate that heterogeneous expression of NNAT is also a feature of the adult human pancreatic islet. Finally, NNAT$^+$ cells were de-enriched for highly connected 'hubs' and, thus, are likelier to belong to the 'follower' population [14]. Interestingly, Ca^{2+} responses to 11 mmol/l glucose were significantly higher in *Nnat*-deficient vs wild-type mouse islets, in contrast to previous findings where differences were not observed in response to 16.7 mmol/l glucose [35]. A similar strong tendency was also seen when comparing NNAT$^+$ vs NNAT$^-$ cells in the same islet in *Nnat*-eGFP reporter mice,

and suggests that NNAT$^+$ cells are less responsive to metabolic stimulation by glucose, in line with their enrichment in a 'follower' subset of cells, and consistent with a role in insulin production rather than glucose detection [14, 15]. The molecular underpinnings of the weaker Ca^{2+} responses are unclear, but do not appear to involve differences in the levels of transcripts encoding *Slc2a2* (*Glut2*) or *Gck*. Moreover, the transcriptome of NNAT$^+$ cells does not show enrichment for genes enriched in 'hub' [15] or 'leader' cells [25].

Interestingly, bimodal expression of *Nnat* was already clearly evident at embryonic stages, with *Nnat*$^+$ beta cells enriched for markers of late-stage beta cell differentiation, as well as *Ins1* and *Ins2* mRNAs. These differences were, however, less marked in the adult islet, though CD24a [7] was more weakly expressed in the NNAT$^+$ population. De-enrichment of markers of other islet cell types (and the immaturity marker *Cd81*) was also a common feature of both embryonic and adult NNAT$^+$ beta cells. Interestingly, both embryonic and adult NNAT$^+$ beta cells were enriched for *Npy*, suggesting that these cells were not fully matured. NNAT$^+$ beta cells, however, had significantly higher insulin content, suggesting a possible, at least partial, overlap with the recently described 'CD63^{hi}' population [23], and the 'β_{HI}' population described in reference [7].

Our work also provides evidence that the epigenome controls the fate of specific beta cell subpopulations. CpG methylation plays a crucial role in early beta cell developmental maturation, including the silencing of 'disallowed' genes such as *Hk1*, *Mct1* (*Slc16a1*) and *Ldha* via DNMT3A [4, 48]. Here we show that islets transition from a state wherein the majority of beta cells are NNAT$^+$ in late embryogenesis to comprising a restricted subpopulation of NNAT$^+$ beta cells by P7. Whether this represents changes at the level of individual beta cells, or the turnover of the NNAT$^+$ population and replacement with a largely NNAT$^-$ population, was not determined, and would require investigation using other approaches, including fate mapping (lineage tracing).

Adult NNAT$^+$ beta cells are virtually unmethylated at the *Nnat* promoter whereas robust promoter methylation was apparent in NNAT$^-$ cells. These findings, and the fact that the *Nnat* promoter is differentially methylated between sperm and oocytes (see the Results), indicate that promoter methylation during this transition is likely to be acquired on the paternal allele (from which *Nnat* is selectively expressed via genomic imprinting). Our studies also show that specific deletion of the de novo methyltransferase DNMT3A at the pancreatic progenitor stage resulted in partial loss of NNAT-based beta cell heterogeneity. Thus, DNA methylation modulates restricted NNAT expression in specific beta cells during early maturation.

Might these findings be relevant for the pathogenesis of type 2 diabetes? Whether demethylation of the second DMR at the *Nnat* locus may occur in this disease is an interesting possibility which remains to be explored. In rodents, even mild hyperglycaemia deregulates *Nnat* expression alongside that of several other critical beta cell identity genes [52], and we describe here a significant reduction of NNAT$^+$ beta cells in *db/db* mice. Moreover, altered CpG methylation is a common observation in islets from individuals with diabetes at imprinted and non-imprinted loci (reviewed in [18, 32]).

In conclusion, the present work demonstrates how an effector gene in pancreatic beta cells, *NNAT/Nnat*, is controlled at the level of the epigenome (DNA methylome), contributing to a functional hierarchy between cells. Chemical modification of the epigenome may in future provide an attractive therapeutic angle not only for beta cell replacement or regeneration [53] but also to modulate beta cell function and cell–cell connectivity in type 2 diabetes.

Supplementary Information The online version contains peer-reviewed but unedited supplementary material available at https://doi.org/10.1007/s00125-024-06123-6.

Acknowledgements We thank the LMS/NIHR Imperial Biomedical Research Centre Flow Cytometry Facility and the MRC LMS Genomics Facility for the support. Some of the data were presented as an abstract at the Society for Endocrinology BES meeting and the 59th EASD Annual Meeting, both in 2023. The graphical abstract and Fig. 5g were created with BioRender.com.

Data availability RNA-seq data are available from the GEO under accession number GSE249659. The mass spectrometry proteomics data have been deposited to the ProteomeXchange Consortium via the PRIDE partner repository with the dataset identifier PXD048465. ImageJ scripts and CellProfiler pipelines can be made available upon reasonable request. Pseudo-time analysis scripts are available via GitHub using the link https://github.com/aosakwe/Pseudotime_Analysis_MouseIslets. Transcriptomic data for *ob/ob* mice can be obtained from a publicly available source from the Alan Attie laboratory (http://diabetes.wisc.edu/search).

Funding AMa received a Summer Studentship in the SJM laboratory from the Society for Endocrinology. AO is supported by training scholarships from the Canadian Institutes of Health Research (CIHR) and the Fonds de recherche du Québec – Santé (FRQS). SSV is a CIRM postdoctoral scholar supported by the California Institute for Regenerative Medicine (EDU4-12772). YA is supported by the Singapore Ministry of Education Academic Research Fund Tier 2 (MOE-T2EP30221-0003). PM and MS have been supported by the European Union, Next Generation EU, through the Italian Ministry of University and Research under PNRR - M4C2-1.3, Project PE_00000019 HEAL ITALIA. SD is supported by the National Institutes of Health (NIH) (R01DK120523), by the Wanek Family Foundation to Cure Type 1 Diabetes and by start-up funds from the City of Hope. This work was also supported by a Wellcome Trust Project Grant (093082/Z/10/Z) to DJW and by funding from the Medical Research Council (MRC) to DJW (MC-A654-5QB40). GAR was supported by a Wellcome Trust Investigator award (212625/Z/18/Z), a UKRI-MRC Programme grant (MR/R022259/1), an NIH-NIDDK project grant (R01DK135268), a CIHR-JDRF Team grant (CIHR-IRSC TDP-186358 and JDRF 4-SRA-2023-1182-S-N), CRCHUM start-up funds and an Innovation Canada John R. Evans Leader Award (CFI 42649). GAR and PM received funding from the European Union's Horizon 2020 research and innovation programme via the Innovative Medicines Initiative 2 Joint Undertaking under grant agreement no. 115881 (RHAPSODY). Work in the SJM laboratory was supported by a Wellcome Trust ISSF Fellowship (204834/Z/16/Z, award no. RSRO_67869) and by a Society for Endocrinology Early Career Grant (WREC_P93206) and Small Equipment Grant (WREC_NCP239).

Authors' relationships and activities PM is a member of the Editorial Board of *Diabetologia*. GAR has received grant funding from and is a consultant for Sun Pharmaceuticals Inc. The authors declare that there are no other relationships or activities that might bias, or be perceived to bias, their work.

Contribution statement SJM and GAR designed the research. VY, FY, AMa, SK, AO, SB, SSV, PC, SMT, KC, EG, NP, MS, ZS, LM, CDL, MT, GO, LD-S, XW, YH, AMo, JE, BP, ND, CW, PH, PS, HK, YA, PM, RS, SD, DJW and SJM performed and interpretated experiments and analyses. PH, PM, RS, SD and DJW contributed new reagents/analytical tools. SJM and GAR drafted and/or wrote the manuscript. SJM, SD, DJW and GAR provided funding. SJM and GAR supervised the work. SJM serves as the guarantor of this work. All authors critically reviewed and approved the manuscript according to the ICMJE criteria.

Open Access This article is licensed under a Creative Commons Attribution 4.0 International License, which permits use, sharing, adaptation, distribution and reproduction in any medium or format, as long as you give appropriate credit to the original author(s) and the source, provide a link to the Creative Commons licence, and indicate if changes were made. The images or other third party material in this article are included in the article's Creative Commons licence, unless indicated otherwise in a credit line to the material. If material is not included in the article's Creative Commons licence and your intended use is not permitted by statutory regulation or exceeds the permitted use, you will need to obtain permission directly from the copyright holder. To view a copy of this licence, visit http://creativecommons.org/licenses/by/4.0/.

References

1. Rutter GA, Pullen TJ, Hodson DJ, Martinez-Sanchez A (2015) Pancreatic β-cell identity, glucose sensing and the control of insulin secretion. Biochem J 466(2):203–218. https://doi.org/10.1042/BJ20141384
2. Salinno C, Cota P, Bastidas-Ponce A, Tarquis-Medina M, Lickert H, Bakhti M (2019) β-cell maturation and identity in health and disease. Int J Mol Sci 20(21):5417. https://doi.org/10.3390/ijms20215417
3. Hoffman BG, Robertson G, Zavaglia B et al (2010) Locus co-occupancy, nucleosome positioning, and H3K4me1 regulate the functionality of FOXA2-, HNF4A-, and PDX1-bound loci in islets and liver. Genome Res 20(8):1037–1051. https://doi.org/10.1101/gr.104356.109
4. Dhawan S, Tschen SI, Zeng C et al (2015) DNA methylation directs functional maturation of pancreatic β cells. J Clin Invest 125(7):2851–2860. https://doi.org/10.1172/JCI79956
5. Lu TT, Heyne S, Dror E et al (2018) The polycomb-dependent epigenome controls β cell dysfunction, dedifferentiation, and diabetes. Cell Metab 27(6):1294-1308 e1297. https://doi.org/10.1016/j.cmet.2018.04.013
6. Parveen N, Wang JK, Bhattacharya S et al (2023) DNA methylation dependent restriction of tyrosine hydroxylase contributes to pancreatic β-cell heterogeneity. Diabetes 72(5):575–589. https://doi.org/10.2337/db22-0506
7. Dror E, Fagnocchi L, Wegert V et al (2023) Epigenetic dosage identifies two major and functionally distinct β cell subtypes. Cell Metab 35(5):821-836 e827. https://doi.org/10.1016/j.cmet.2023.03.008
8. Salomon D, Meda P (1986) Heterogeneity and contact-dependent regulation of hormone secretion by individual B cells. Exp Cell Res 162(2):507–520. https://doi.org/10.1016/0014-4827(86)90354-x
9. Bosco D, Meda P (1991) Actively synthesizing β-cells secrete preferentially after glucose stimulation. Endocrinology 129(6):3157–3166. https://doi.org/10.1210/endo-129-6-3157
10. Dorrell C, Schug J, Canaday PS et al (2016) Human islets contain four distinct subtypes of β cells. Nat Commun 7:11756. https://doi.org/10.1038/ncomms11756
11. Wang YJ, Schug J, Won KJ et al (2016) Single-cell transcriptomics of the human endocrine pancreas. Diabetes 65(10):3028–3038. https://doi.org/10.2337/db16-0405
12. Segerstolpe A, Palasantza A, Eliasson P et al (2016) Single-cell transcriptome profiling of human pancreatic islets in health and type 2 diabetes. Cell Metab 24(4):593–607. https://doi.org/10.1016/j.cmet.2016.08.020
13. Camunas-Soler J, Dai XQ, Hang Y et al (2020) Patch-seq links single-cell transcriptomes to human islet dysfunction in diabetes. Cell Metab 31(5):1017-1031 e1014. https://doi.org/10.1016/j.cmet.2020.04.005
14. Johnston NR, Mitchell RK, Haythorne E et al (2016) Beta cell hubs dictate pancreatic islet responses to glucose. Cell Metab 24(3):389–401. https://doi.org/10.1016/j.cmet.2016.06.020
15. Salem V, Silva LD, Suba K et al (2019) Leader β-cells coordinate Ca^{2+} dynamics across pancreatic islets in vivo. Nat Metab 1(6):615–629. https://doi.org/10.1038/s42255-019-0075-2
16. Bader E, Migliorini A, Gegg M et al (2016) Identification of proliferative and mature β-cells in the islets of Langerhans. Nature 535(7612):430–434. https://doi.org/10.1038/nature18624
17. Westacott MJ, Ludin NWF, Benninger RKP (2017) Spatially organized β-cell subpopulations control electrical dynamics across islets of Langerhans. Biophys J 113(5):1093–1108. https://doi.org/10.1016/j.bpj.2017.07.021
18. Chabosseau P, Rutter GA, Millership SJ (2021) Importance of both imprinted genes and functional heterogeneity in pancreatic beta cells: is there a link? Int J Mol Sci 22(3):1000. https://doi.org/10.3390/ijms22031000
19. Karaca M, Castel J, Tourrel-Cuzin C et al (2009) Exploring functional β-cell heterogeneity in vivo using PSA-NCAM as a specific marker. PLoS One 4(5):e5555. https://doi.org/10.1371/journal.pone.0005555
20. Salinno C, Buttner M, Cota P et al (2021) CD81 marks immature and dedifferentiated pancreatic β-cells. Mol Metab 49:101188. https://doi.org/10.1016/j.molmet.2021.101188
21. Muraro MJ, Dharmadhikari G, Grun D et al (2016) A single-cell transcriptome atlas of the human pancreas. Cell Syst 3(4):385-394 e383. https://doi.org/10.1016/j.cels.2016.09.002
22. Rodnoi P, Rajkumar M, Moin ASM, Georgia SK, Butler AE, Dhawan S (2017) Neuropeptide Y expression marks partially differentiated β cells in mice and humans. JCI Insight 2(12):e94005. https://doi.org/10.1172/jci.insight.94005
23. Rubio-Navarro A, Gomez-Banoy N, Stoll L et al (2023) A beta cell subset with enhanced insulin secretion and glucose metabolism is reduced in type 2 diabetes. Nat Cell Biol 25(4):565–578. https://doi.org/10.1038/s41556-023-01103-1
24. van der Meulen T, Mawla AM, DiGruccio MR et al (2017) Virgin beta cells persist throughout life at a neogenic niche within pancreatic islets. Cell Metab 25(4):911-926 e916. https://doi.org/10.1016/j.cmet.2017.03.017
25. Chabosseau P, Yong F, Delgadillo-Silva LF et al (2023) Molecular phenotyping of single pancreatic islet leader beta cells by "Flash-Seq." Life Sci 316:121436. https://doi.org/10.1016/j.lfs.2023.121436
26. Kravets V, Dwulet JM, Schleicher WE et al (2022) Functional architecture of pancreatic islets identifies a population of first

responder cells that drive the first-phase calcium response. PLoS Biol 20(9):e3001761. https://doi.org/10.1371/journal.pbio.3001761
27. Nasteska D, Fine NHF, Ashford FB et al (2021) PDX1^{LOW} MAFA^{LOW} β-cells contribute to islet function and insulin release. Nat Commun 12(1):674. https://doi.org/10.1038/s41467-020-20632-z
28. Wang G, Chiou J, Zeng C et al (2023) Integrating genetics with single-cell multiomic measurements across disease states identifies mechanisms of beta cell dysfunction in type 2 diabetes. Nat Genet 55(6):984–994. https://doi.org/10.1038/s41588-023-01397-9
29. Katsuta H, Aguayo-Mazzucato C, Katsuta R et al (2012) Subpopulations of GFP-marked mouse pancreatic β-cells differ in size, granularity, and insulin secretion. Endocrinology 153(11):5180–5187. https://doi.org/10.1210/en.2012-1257
30. Xin Y, Dominguez Gutierrez G, Okamoto H et al (2018) Pseudotime ordering of single human β-cells reveals states of insulin production and unfolded protein response. Diabetes 67(9):1783–1794. https://doi.org/10.2337/db18-0365
31. Millership SJ, Van de Pette M, Withers DJ (2019) Genomic imprinting and its effects on postnatal growth and adult metabolism. Cell Mol Life Sci 76(20):4009–4021. https://doi.org/10.1007/s00018-019-03197-z
32. Villanueva-Hayes C, Millership SJ (2021) Imprinted genes impact upon beta cell function in the current (and potentially next) generation. Front Endocrinol (Lausanne) 12:660532. https://doi.org/10.3389/fendo.2021.660532
33. Ferguson-Smith AC (2011) Genomic imprinting: the emergence of an epigenetic paradigm. Nat Rev Genet 12(8):565–575. https://doi.org/10.1038/nrg3032
34. John RM, Lefebvre L (2011) Developmental regulation of somatic imprints. Differentiation 81(5):270–280. https://doi.org/10.1016/j.diff.2011.01.007
35. Millership SJ, Da Silva Xavier G, Choudhury AI et al (2018) Neuronatin regulates pancreatic beta cell insulin content and secretion. J Clin Invest 128(8):3369–3381. https://doi.org/10.1172/JCI120115
36. Vrang N, Meyre D, Froguel P et al (2010) The imprinted gene neuronatin is regulated by metabolic status and associated with obesity. Obesity (Silver Spring) 18(7):1289–1296. https://doi.org/10.1038/oby.2009.361
37. Dalgaard K, Landgraf K, Heyne S et al (2016) Trim28 haploinsufficiency triggers bi-stable epigenetic obesity. Cell 164(3):353–364. https://doi.org/10.1016/j.cell.2015.12.025
38. Millership SJ, Tunster SJ, Van de Pette M et al (2018) Neuronatin deletion causes postnatal growth restriction and adult obesity in 129S2/Sv mice. Mol Metab 18:97–106. https://doi.org/10.1016/j.molmet.2018.09.001
39. Byrnes LE, Wong DM, Subramaniam M et al (2018) Lineage dynamics of murine pancreatic development at single-cell resolution. Nat Commun 9(1):3922. https://doi.org/10.1038/s41467-018-06176-3
40. Sasaki S, Lee MYY, Wakabayashi Y et al (2022) Spatial and transcriptional heterogeneity of pancreatic beta cell neogenesis revealed by a time-resolved reporter system. Diabetologia 65(5):811–828. https://doi.org/10.1007/s00125-022-05662-0
41. Sachs S, Bastidas-Ponce A, Tritschler S et al (2020) Targeted pharmacological therapy restores β-cell function for diabetes remission. Nat Metab 2(2):192–209. https://doi.org/10.1038/s42255-020-0171-3
42. Tritschler S, Thomas M, Bottcher A et al (2022) A transcriptional cross species map of pancreatic islet cells. Mol Metab 66:101595. https://doi.org/10.1016/j.molmet.2022.101595
43. Herrera PL (2000) Adult insulin- and glucagon-producing cells differentiate from two independent cell lineages. Development 127(11):2317–2322. https://doi.org/10.1242/dev.127.11.2317
44. Luche H, Weber O, Nageswara Rao T, Blum C, Fehling HJ (2007) Faithful activation of an extra-bright red fluorescent protein in "knock-in" Cre-reporter mice ideally suited for lineage tracing studies. Eur J Immunol 37(1):43–53. https://doi.org/10.1002/eji.200636745
45. Parton LE, McMillen PJ, Shen Y et al (2006) Limited role for SREBP-1c in defective glucose-induced insulin secretion from Zucker diabetic fatty rat islets: a functional and gene profiling analysis. Am J Physiol Endocrinol Metab 291(5):E982-994. https://doi.org/10.1152/ajpendo.00067.2006
46 Herman JS, Sagar, Grun D (2018) FateID infers cell fate bias in multipotent progenitors from single-cell RNA-seq data. Nat Methods 15(5):379–386. https://doi.org/10.1038/nmeth.4662
47. Jima DD, Skaar DA, Planchart A et al (2022) Genomic map of candidate human imprint control regions: the imprintome. Epigenetics 17(13):1920–1943. https://doi.org/10.1080/15592294.2022.2091815
48. Pullen TJ, Huising MO, Rutter GA (2017) Analysis of purified pancreatic islet beta and alpha cell transcriptomes reveals 11β-hydroxysteroid dehydrogenase (Hsd11b1) as a novel disallowed gene. Front Genet 8:41. https://doi.org/10.3389/fgene.2017.00041
49. Georgiadou E, Muralidharan C, Martinez M et al (2022) Mitofusins Mfn1 and Mfn2 are required to preserve glucose- but not incretin-stimulated β-cell connectivity and insulin secretion. Diabetes 71(7):1472–1489. https://doi.org/10.2337/db21-0800
50. Ivanova E, Chen JH, Segonds-Pichon A, Ozanne SE, Kelsey G (2012) DNA methylation at differentially methylated regions of imprinted genes is resistant to developmental programming by maternal nutrition. Epigenetics 7(10):1200–1210. https://doi.org/10.4161/epi.22141
51. Van de Pette M, Abbas A, Feytout A et al (2017) Visualizing changes in Cdkn1c expression links early-life adversity to imprint mis-regulation in adults. Cell Rep 18(5):1090–1099. https://doi.org/10.1016/j.celrep.2017.01.010
52. Ebrahimi AG, Hollister-Lock J, Sullivan BA, Tsuchida R, Bonner-Weir S, Weir GC (2020) Beta cell identity changes with mild hyperglycemia: implications for function, growth, and vulnerability. Mol Metab 35:100959. https://doi.org/10.1016/j.molmet.2020.02.002
53. Ou K, Yu M, Moss NG et al (2019) Targeted demethylation at the CDKN1C/p57 locus induces human β cell replication. J Clin Invest 129(1):209–214. https://doi.org/10.1172/JCI99170

Publisher's Note Springer Nature remains neutral with regard to jurisdictional claims in published maps and institutional affiliations.

Authors and Affiliations

Vanessa Yu[1] · Fiona Yong[1,2] · Angellica Marta[1] · Sanjay Khadayate[3] · Adrien Osakwe[4] · Supriyo Bhattacharya[5] · Sneha S. Varghese[6] · Pauline Chabosseau[1] · Sayed M. Tabibi[1] · Keran Chen[1,7] · Eleni Georgiadou[1] · Nazia Parveen[6] · Mara Suleiman[8] · Zoe Stamoulis[1,9] · Lorella Marselli[8] · Carmela De Luca[8] · Marta Tesi[8] · Giada Ostinelli[10] · Luis Delgadillo-Silva[10] · Xiwei Wu[5] · Yuki Hatanaka[3,11] · Alex Montoya[3] · James Elliott[3] · Bhavik Patel[3] · Nikita Demchenko[3,12] · Chad Whilding[3] · Petra Hajkova[3,11] · Pavel Shliaha[3] · Holger Kramer[3] · Yusuf Ali[13,14,15] · Piero Marchetti[8] · Robert Sladek[4,16] · Sangeeta Dhawan[6] · Dominic J. Withers[3,11] · Guy A. Rutter[1,10,2] · Steven J. Millership[1]

✉ Guy A. Rutter
g.rutter@imperial.ac.uk; guy.rutter@umontreal.ca

✉ Steven J. Millership
s.millership@imperial.ac.uk

1 Department of Metabolism, Digestion and Reproduction, Faculty of Medicine, Imperial College London, London, UK

2 Lee Kong Chian School of Medicine, Nanyang Technological University, Singapore, Republic of Singapore

3 MRC Laboratory of Medical Sciences, London, UK

4 Quantitative Life Sciences Program, McGill University, Montréal, QC, Canada

5 Department of Computational and Quantitative Medicine, Beckman Research Institute, City of Hope, Duarte, CA, USA

6 Department of Translational Research and Cellular Therapeutics, Arthur Riggs Diabetes and Metabolism Research Institute, City of Hope, Duarte, CA, USA

7 Present Address: Biomedical Research Centre, School of Biological Sciences, University of East Anglia, Norwich, UK

8 Department of Clinical and Experimental Medicine, and AOUP Cisanello University Hospital, University of Pisa, Pisa, Italy

9 Present Address: Medical Sciences Division, University of Oxford, Oxford, UK

10 CHUM Research Center and Faculty of Medicine, University of Montréal, Montréal, QC, Canada

11 Institute of Clinical Sciences, Faculty of Medicine, Imperial College London, London, UK

12 Present Address: Imaging Resource Facility, Research Operations, St George's, University of London, London, UK

13 Nutrition, Metabolism and Health Programme & Centre for Microbiome Medicine, Lee Kong Chian School of Medicine, Nanyang Technological University Singapore, Singapore, Republic of Singapore

14 Singapore Eye Research Institute (SERI), Singapore General Hospital, Singapore, Republic of Singapore

15 Clinical Research Unit, Khoo Teck Puat Hospital, National Healthcare Group, Singapore, Republic of Singapore

16 Departments of Medicine and Human Genetics, McGill University, Montréal, QC, Canada